NRIAG JOURNAL OF ASTRONOMY AND GEOPHYSICS
2020, VOL. 9, NO. 1, 106–115
https://doi.org/10.1080/20909977.2020.1723199

Registration-based change detection for SAR images

Alshimaa Y. Abo Gharbia[a], Mohamed Amin[b], Ashraf E. Mousa[a], Nadia AbouAly[a], Ghada M. El Banby[c] and Fathi E. Abd El-Samie[d]

[a]Geodynamic Department, National Research Institute of Astronomy and Geophysics, Helwan, Egypt; [b]Mathematics and Computer Science Department, Menoufia University, Shebin El-koom, Egypt; [c]Department of Industrial Electronics and Control Engineering, Menoufia University, Menouf, Egypt; [d]Department of Electronics and Electrical Communications Engineering, Menoufia University, Menouf, Egypt

ABSTRACT

This paper presents an efficient change detection approach for Synthetic Aperture Radar (SAR) images. The basic idea of this approach is to use the log ratio of the two images for change detection after being registered with Scale-Invariant Feature Transform (SIFT). These two images are a reference image and another image for the same area acquired at a different time. The log ratio variations include changes in certain areas corresponding to the natural changes in the test image. Usually, SAR images contain some sort of noise. So, there is a need for a denoising process prior to estimating the log ratio to enhance the change detection results. A segmentation process is performed on the test image based on the log ratio values. Large values in the log ratio image correspond to detected changes in the test image. Simulation results on SAR images for a region of Jeddah demonstrate the success of the proposed approach.

ARTICLE HISTORY
Received 21 July 2019
Revised 9 January 2020
Accepted 23 January 2020

KEYWORDS
Registration; SIFT; SAR; change detection

1. Introduction

Remote sensing uses the satellite or aircraft-based sensor technologies to survey the Earth. There are two types of remote sensing: "active" and "passive". In active remote sensing, a signal is sent by the satellite or aircraft and the echo is received by a sensor. In passive remote sensing, the reflection of sunlight is received by the sensor. We can obtain high-resolution spotlight SAR images from TerraSAR-X radar.

Generally, the input in image processing applications is an image and the output is a part of that image or its properties. Change detection in SAR imaging aims to determine the changes that may have happened over the same area at different times. The SAR system has been used in several applications such as agricultural surveys, damage assessment, forest observations, environmental observations, and urban studies. However, as the SAR images suffer from speckle noise, this leads to inaccurate change detection.

Real-world SAR applications are diverse. The SAR images are used for sorting and discovering land cover. They save time and high cost of field surveys. They are used also for observation of the forest tree species, for defining urban patterns, for defining the extent of floods, and for pinpointing the area of deforestation (Wang et al. 2016). Detecting changes in land-cover is one of the most important fundamentals of remote sensing image analysis. In remote sensing, change detection shows changes on land cover by surveying them at different times.

Change detection process in SAR images usually has two phases: difference detection from images using several types of operations and classification of images with or without changes based on supervised or unsupervised techniques (Bovolo and Bruzzone, 2005), (Celik, 2010), (Jia et al., 2018). The determination of changes is usually based on a ratio operator, which is sensitive to radiometric and calibration errors. Moreover, speckle noise in SAR images may affect the performance. Minimisation of the effect of speckle noise can be performed based on a log ratio operator (Das et al. 2016).

By applying a spatial filter, we can reduce the speckle noise effect on the image. Radar speckle is roughly multiplicative noise. The range of the random brightness deviations increases with the average grey level of a local area (ftp.microimages.com). By using either the entire image or the local neighbourhood of the filter window, variations in actual brightness can reflect the noise range. The objective is to reduce the speckle noise in uniform regions by some kind of averaging while conserving the brightness variations that exist at the boundaries between areas of varying brightness. The radar filters are better than simple low-pass or median filters for noise reduction. Some of these radar filters have variables that can be modified to optimise the results (www.gisteam.de).

In the previous work, the change detection from SAR images is based on pixel information. The

CONTACT Alshimaa Y. Abo gharbia alshimaayousre@gmail.com Geodynamic Department, National Research Institute of Astronomy and Geophysics, Helwan 11421, Egypt

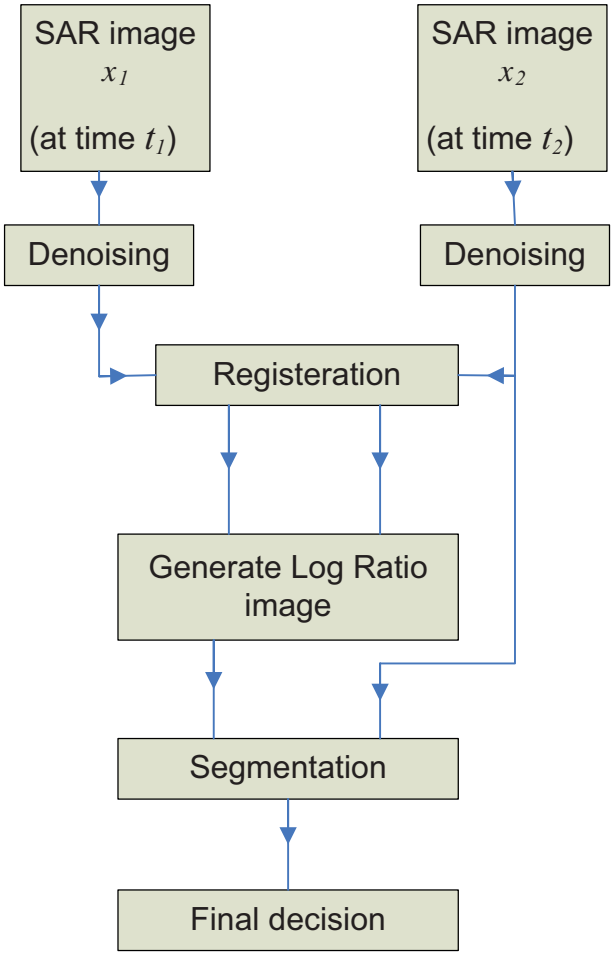

Figure 1. General scheme diagram of the proposed change detection approach.

traditional methods depend on pixel comparison. They subtract the two multi-temporal images. The SIFT has been used to determine the blob-like structures in images using log ratio images to detect the changes (Wang et al. 2016). Another method used log ratio and mean ratio to obtain a difference image. The authors used *k*-means clustering for segmentation (Das et al. 2016). A improved fuzzy c-means algorithm was used to classify the difference map to generate the resulting change detection map (Ronghua Shang et al. 2019).

The basic idea of this paper is to use the log ratio of the two images used for change detection after being registered with SIFT. The log ratio variations include changes in certain areas. Usually, SAR images contain some sort of noise. So, there is a need for a denoising process, which is performed as an initial stage in the proposed system.

2. Proposed approach

The proposed framework is to obtain a change detection map from two SAR images for the same area as illustrated in Figure 1. Assume that we have two SAR images:

$$x_1 = \{x_1(i,j)|1 \le i \le Y, 1 \le j \le Z\}, x_2 = \{x_2(i,j)|1 \le i \le H, 1 \le J \le K\},$$

where x_1 has a size YZ and x_2 has a size HK, each acquired for the same area, but at different times t_1 and t_2, one of them is a reference for the other. The steps of the proposed approach are as follows:

(1) Acquisition of two SAR images with the same scale and the same orientation: a reference image and a test image after a period of time.
(2) Generation of the log ratio image x.
(3) Segmentation of the test image.
(4) Change detection map generation.

2.1. Registration of the two SAR images

Registration is a very important step to be performed on the test image to have the same scale and orientation as the reference image. By applying the SIFT technique, we obtain the feature keypoints of both images. We estimate gradient magnitude and direction around each keypoint. Hence, we determine the main orientation in an area around the keypoint. We

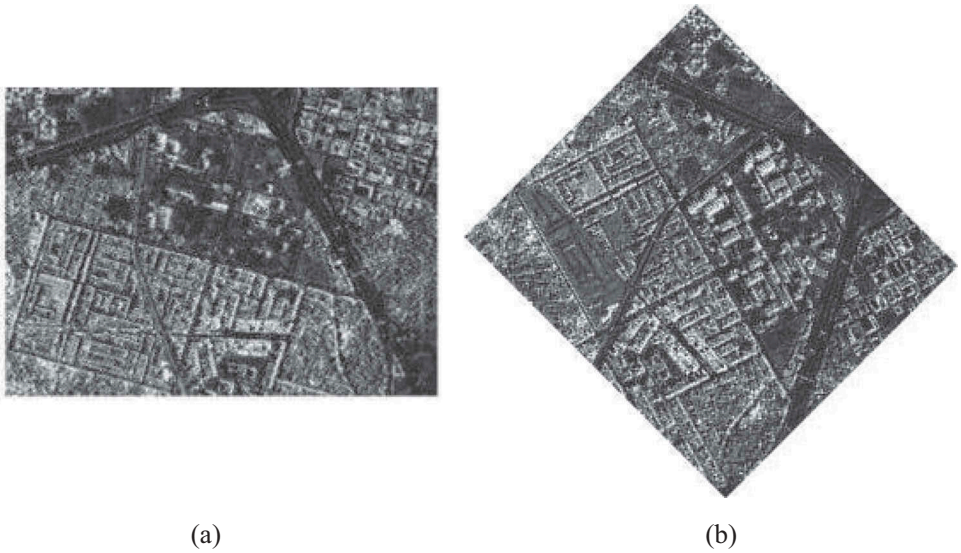

(a) (b)

Figure 2. Two SAR images having different orientations and scales, (a) SAR image1, (b) SAR image2.

specify the magnitude and direction corresponding to a keypoint with the formulae (Lowe 2004):

$$m(x,y) = \sqrt{\begin{array}{l}\left((L(x+1,y) - L(x-1,y)\right)^2 \\ +(L(x,y+1) - L(x,y-1))^2)\end{array}} \quad (1)$$

$$\theta = tan^{-1}(L(x,y+1) - L(x,y-1))/ \\ ((L(x+1,y) - L(x-1,y)) \quad (2)$$

where *x,y* are the location coordinates of the keypoint.

The orientation and magnitude are determined for all pixels around the keypoint. We should have the same scale and rotation invariance for the two images, and then create a signature for each keypoint in the two images. For example, we have two images as shown in Figure 2. We apply the two formulae and affine transformation to obtain the same orientation and the same scale as in Figure 3.

2.2. Generation of the log ratio image

The process of change detection between two different images can be implemented by using log ratio operator:

$$x_e = \log(x_1) - \log(x_2) \quad (3)$$

The logarithmic operator attenuates the pixels in the areas of high intensity and enhances the low-intensity pixels.

2.3. Segmentation

We use the Otsu's method for segmentation. The challenging task is choosing the best threshold values.

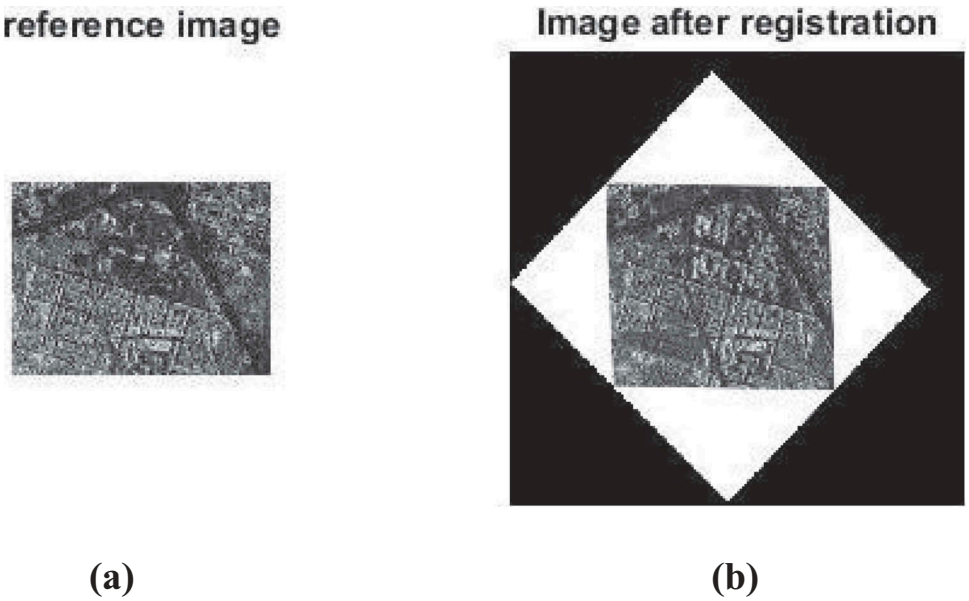

Figure 3. Registration result. (a) Reference image, (b) Image after registration.

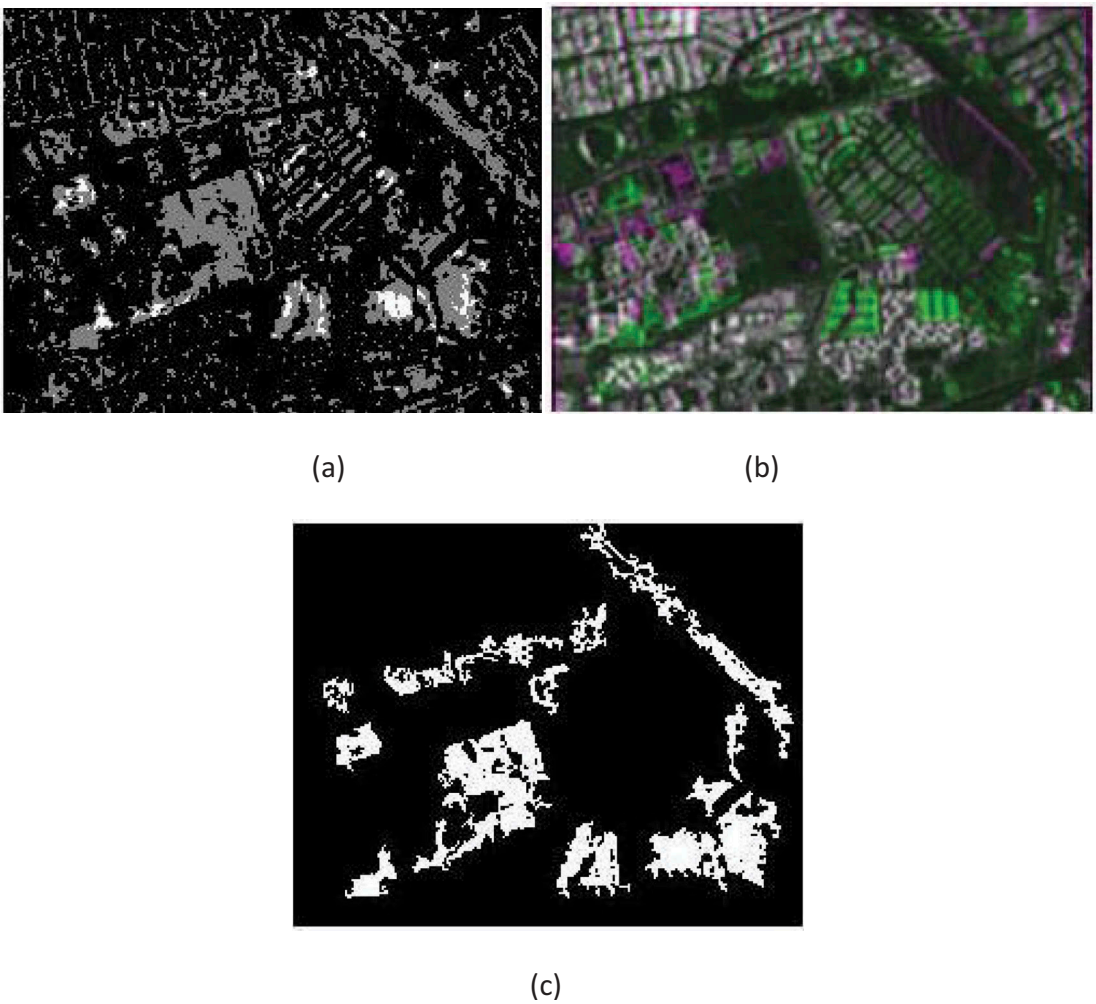

Figure 4. Segmentation of the SAR image (a) Log Ratio image, (b) Pair of SAR images: image1 and image2, (c) Segmentation image.

We determine the change detection map as shown in Figure 4(a). We observe the green colour referring to the changes that exist in the area in the new image and purple colour referring to the destructed buildings as shown in Figure 4(b).

2.4. Obtaining the change map

The change map that illustrates the changes such as new or destroyed buildings is then obtained after the segmentation process.

3. Registration with SIFT

Lowe (2004) presented the SIFT. We can discuss the steps of the SIFT keypoint extraction briefly. **Firstly**, several octaves of the original image are obtained. Sub-sampling by factor 2 is performed for each octave. **Secondly**, images within each octave are processed with a Gaussian filter to perform blurring operation according to the following relation:

$$L(a,b,z) = G(a,b,z) * I(a,b) \quad (4)$$

L is a blurred image, G is the Gaussian Blur operator, I is the SAR image, a,b are the location coordinates, and z is the scale parameter.

Difference of Gaussian (DoG) images are roughly equal to the Laplacian of Gaussian (LoG) images as shown in Figure 5 (Yawalkar et al. 2018). **Thirdly**, we discover the maxima and minima in the DoG images created in the previous step. This is performed by comparing neighbouring pixels in the current scale, scale above and scale below as shown in Figure 6.

The x marks the current pixel. The circles mark the neighbours. In this way, a total of 26 checks are made. The x is marked as a keypoint if it is the greatest or least of all 26 neighbours as shown in Figure 6. Sub-pixel minima/maxima are estimated using the available pixel data. This is performed by the Taylor expansion of the image around the approximate keypoint.

In the image, we perform the subtraction for just one octave as shown in Figure 7. The same thing is performed for all octaves. This generates DoG images of multiple sizes. **Finally**, we can reduce the number of keypoints. SIFT algorithm rejects the keypoints that have low contrast or that are on the edge. We already determine the scale at which the keypoint is discovered

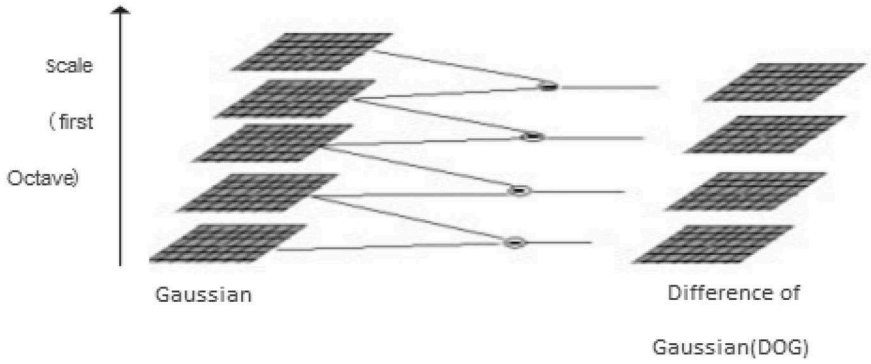

Figure 5. Difference of Gaussian images.

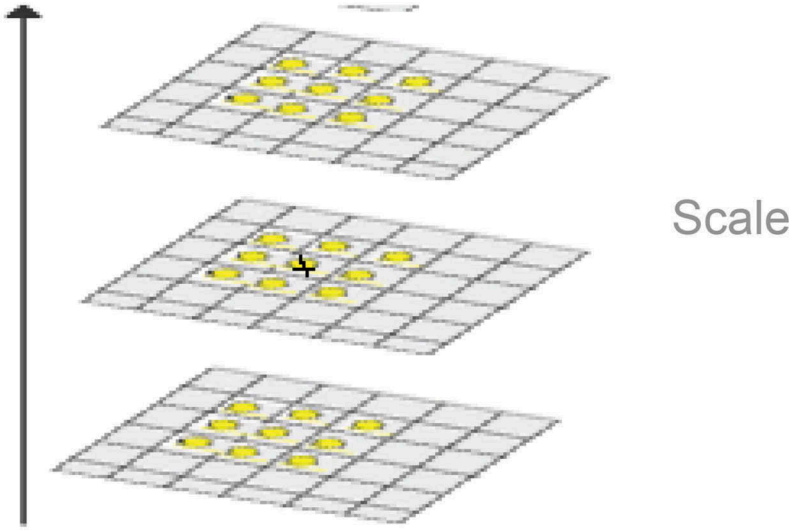

Figure 6. Marked keypoint.

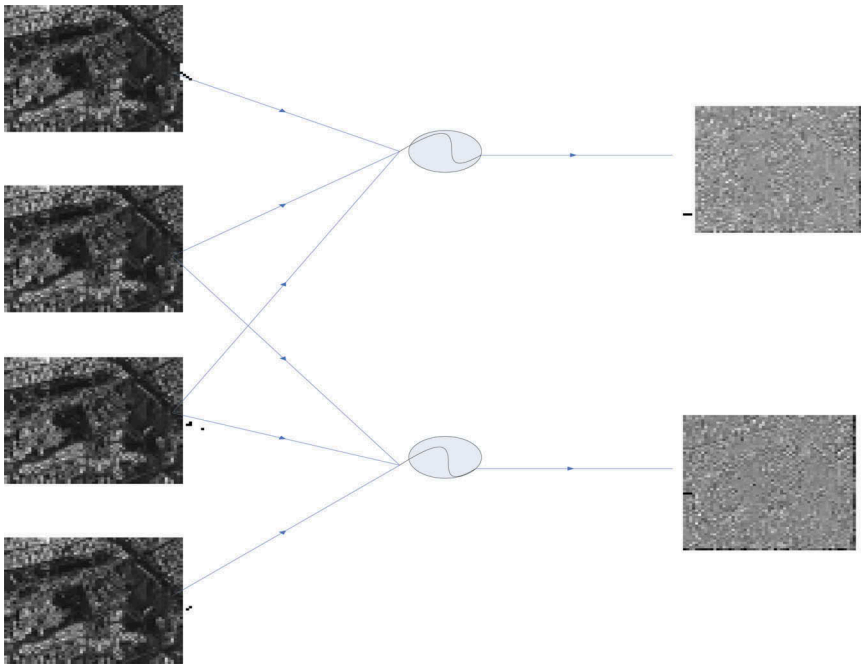

Figure 7. Difference of Gaussian images.

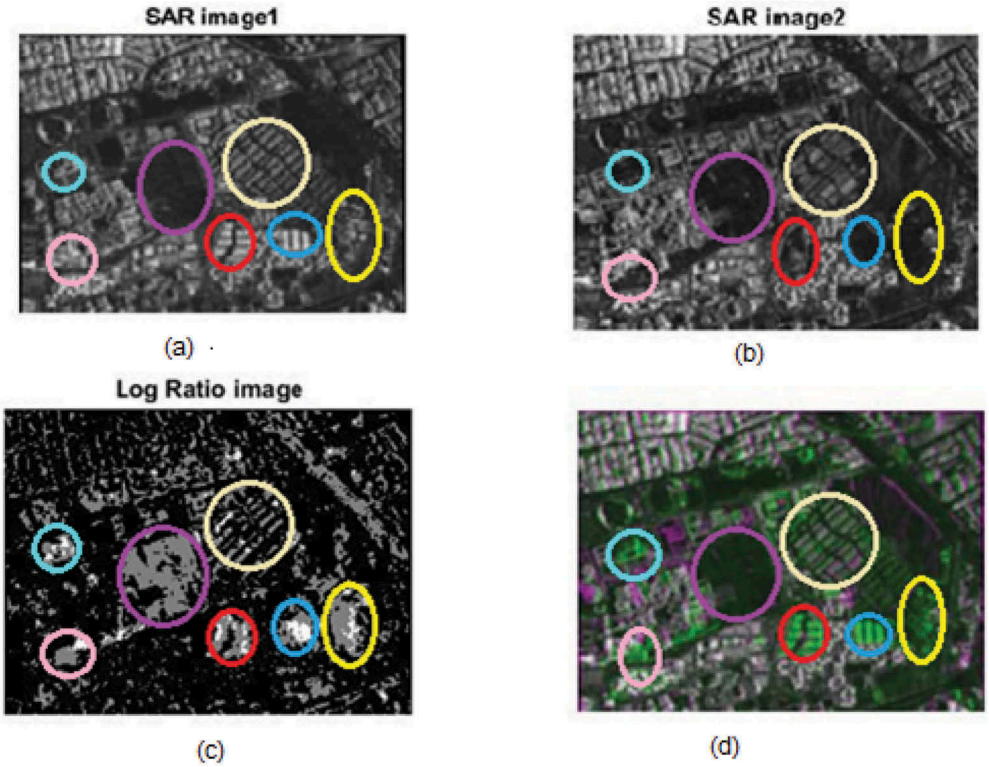

Figure 8. Sample 1(a) SAR image1, (b) SAR image2, (c) Log ratio image, (d) Pair of SAR images: image1 and image2.

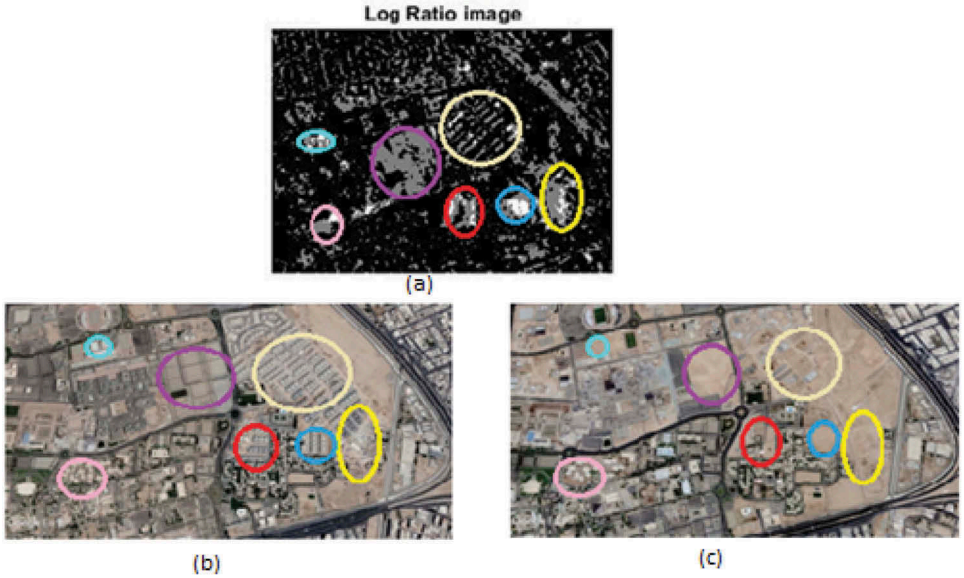

Figure 9. (a) Log ratio image, (b) Google earth image in 2018, (c) Google earth image in 2012.

(it is similar to the scale of the blurred image). The size of the orientation estimation region around the key-point depends on its scale. The larger the scale, the larger the estimation region.

4. Simulation results

Three image sets are used for experiments in this paper, and each set is registered to reduce the error. The three image sets are acquired by German remote sensing TerraSAR-X satellite SAR sensor over Jeddah area in 2012 and 2018.

The first sample has images of size 187 × 236. The second sample has images of size 183 × 245. The third sample has images of size 154 × 132.

Figure 8 shows that the area that changed has circles marked in the SAR image1 in 2018, SAR image2 in 2012, log ratio image and the image that shows a pair of SAR image1 and SAR image2. Figure 9 displays the log ratio image, the Google earth image in 2018 and the Google

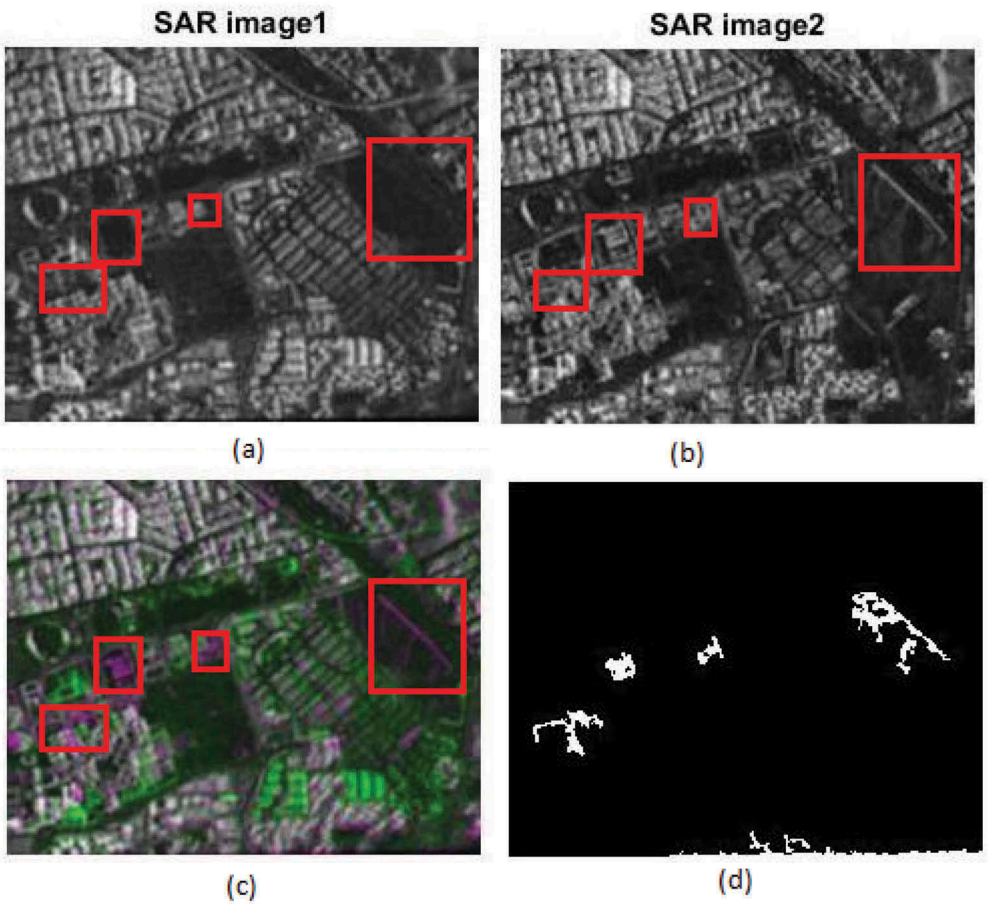

Figure 10. Destroyed buildings. (a) SAR image in 2018, (b) SAR image in 2012, (c) Pair of SAR images: image1 and image2, (d) black and white image.

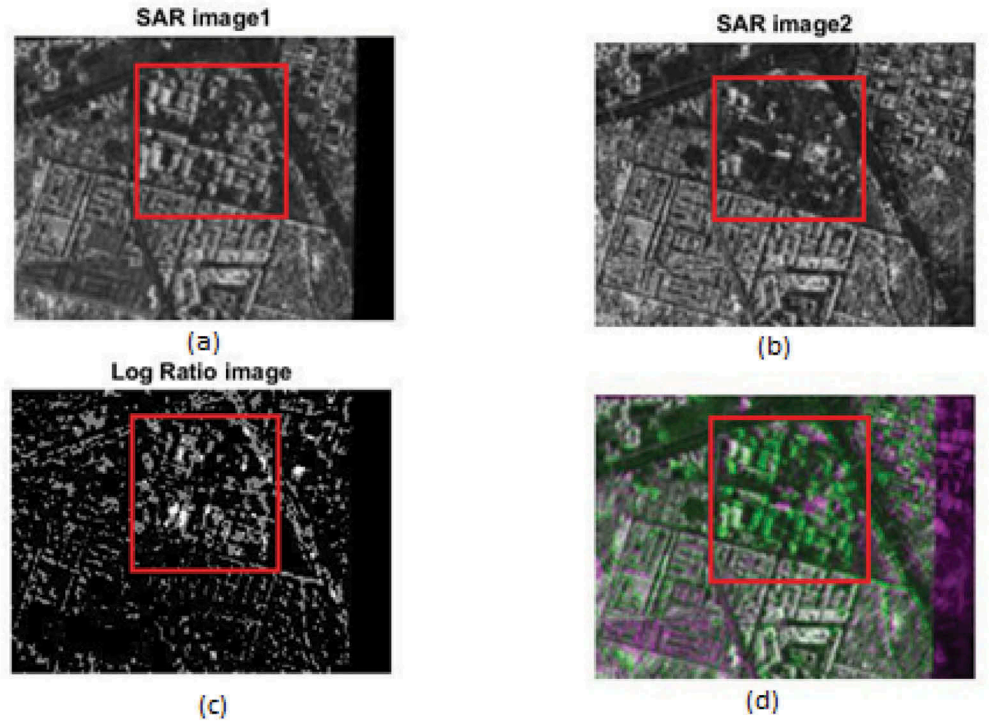

Figure 11. Sample 2.(a) SAR image1, (b) SAR image2, (c) LR image, (d) Pair of SAR images: image1 and image2.

earth image in 2012 to show the extent of change. The circles in the three images show the changes. In another example, we illustrate some destroyed buildings as shown in Figure 10. We observe in Figure 10 the buildings that were built in 2012 and destroyed in 2018 as shown in the red square. Now, we can determine the destroyed

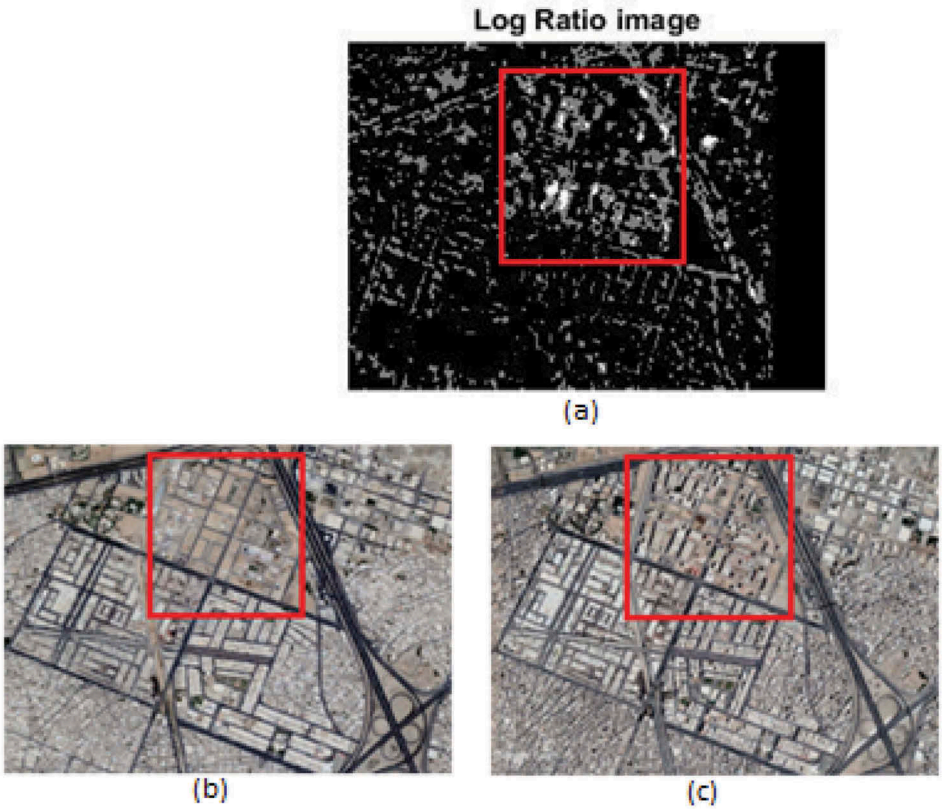

Figure 12. (a) Log ratio image, (b) Google earth image in 2012, (c) Google earth image in 2018.

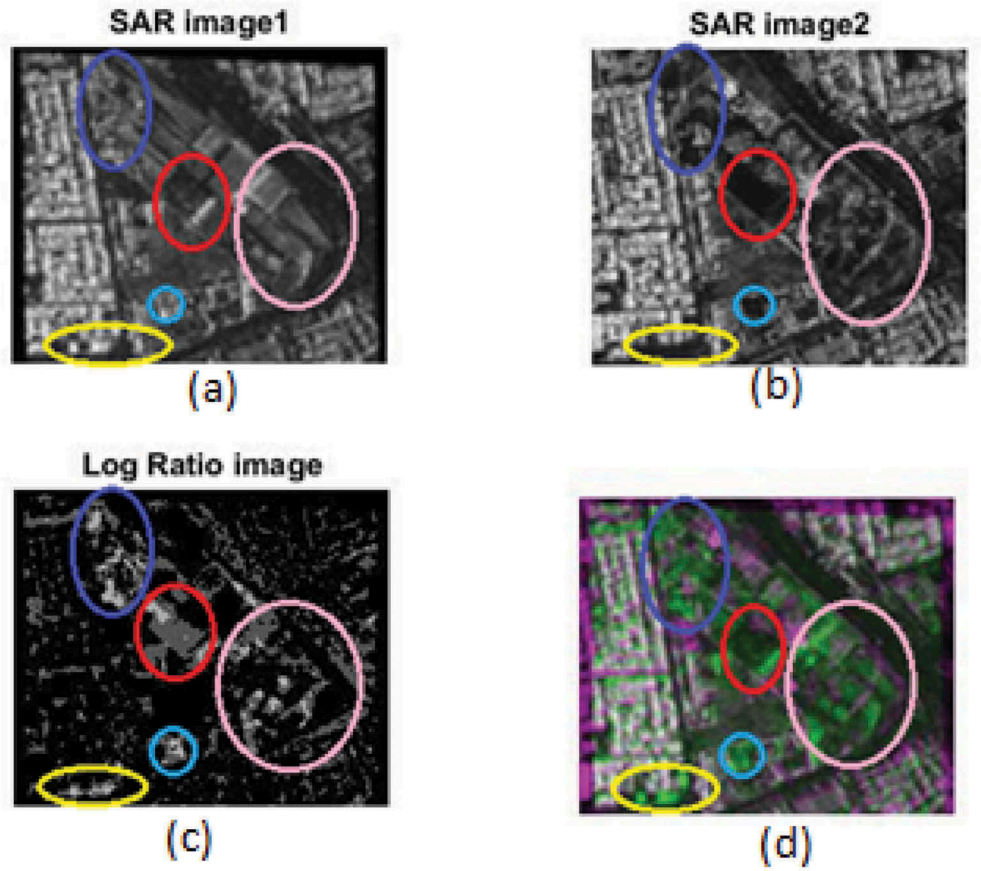

Figure 13. Sample 3, (a) SAR image1, (b) SAR image2, (c) LR image, (d) Pair of SAR images: image1 and image2.

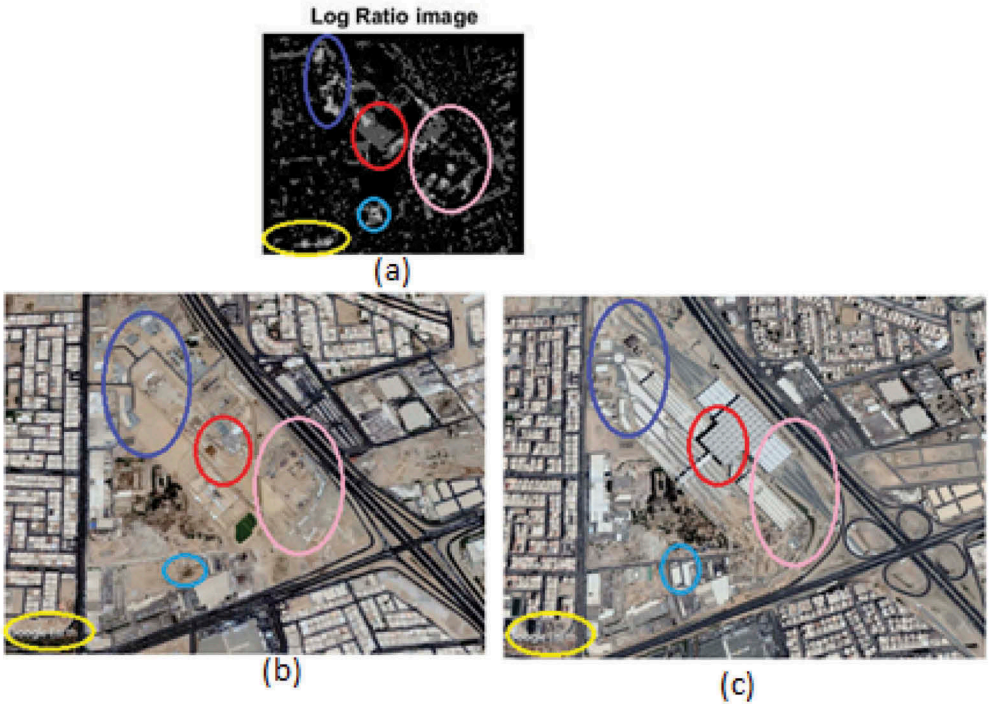

Figure 14. (a) Log ratio image, (b) Google earth image in 2012, (c) Google earth image in 2018.

Table 1. Area ratio of change compared to the original image.

Images	Ratio
Sample 1	3.23%
Sample 2	19.601%
Sample 3	23.65%

buildings in the area after a certain time. From Figure 11, we can observe the area determined by the square in the SAR image1 in 2018, and the SAR image2 in 2012. The log ratio image and that image that shows the pair of SAR image1 and SAR image2 are illustrated. Figure 12 shows

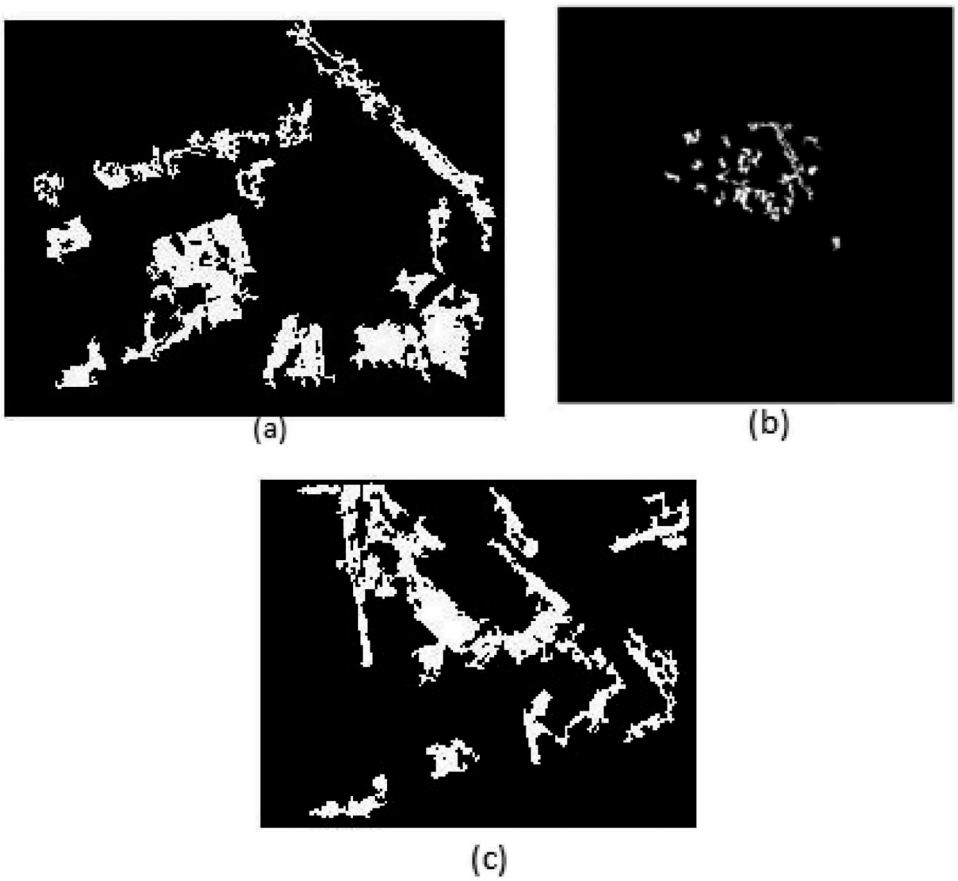

Figure 15. The ground truth image. (a) Ground truth of sample1, (b) Ground truth of sample2, (c) Ground truth of sample3.

the log ratio image, the Google earth image in 2018 and the Google earth image in 2012, which ensure the accuracy of the results. The square shape in each image shows the changes. From Figure 13, we can observe the log ratio image, the Google earth image in 2018 and the Google earth image in 2012. The oval shape in each image shows the changes. From Figure 14, we can observe the log ratio image, the Google earth image in 2018 and the Google earth image in 2012 to make sure of the change detection accuracy. The oval shape in each image shows the changes. We tabulate the values of the evaluation metrics in Table 1 for the images shown in Figure 15. The values in the table show the percentage of new constructions in each region during the period from 2012 to 2018.

5. Conclusion

This paper presented an efficient change detection approach for SAR images. The basic idea of this approach is to begin with SIFT-based registration. After that, Gaussian filtering is applied on the two images to be compared with scale 1. The objective of this step is to reduce the amount of noise. The change detection is performed through a subtraction process in the log domain of un-normalised images to compress the dynamic range of the change to be within the visual range of a normalised image. The proposed approach differs from the state-of-the-art schemes in adopting both registration and log difference together to achieve more accurate change detection results.

Disclosure statement

No potential conflict of interest was reported by the authors.

ORCID

Nadia AbouAly http://orcid.org/0000-0002-8922-2261

Ghada M. El Banby http://orcid.org/0000-0002-7789-9195

References

Bovolo F, Bruzzone L. 2005. A wavelet-based change-detection technique for multitemporal SAR images. International Workshop on the Analysis of Multi-Temporal Remote Sensing Images, 2005; Sydney, Queensland, Australia.

Celik T. 2010. A Bayesian approach to unsupervised multiscale change detection in synthetic aperture radar images. Signal Process. 90:1471–1485.

Das A, Sahi A, Nandini U. 2016. SAR image segmentation for land cover change detection. 2016 Online International Conference on Green Engineering and Technologies (IC-GET); Coimbatore, India.

Jia M, Zhao Z, Huo L, Chen H, Qiu Y. 2018. Incorporating global-local knowledge into expectation-maximization for SAR image change detection. Int J Remote Sens, 734–758.

Lowe DG. 2004 Nov. Distinctive image features from scale-invariant keypoints. Int J Comput Vis. 60 (2):91–110.

Shang R, Xie K, Okoth MA, Jiao L. 2019. Sar image change detection based on mean shift pre-classification and Fuzzy C-means. IGARSS 2019-2019 IEEE International Geoscience and Remote Sensing Symposium; Japan Pacifico, Yokohama.

Wang Y, Du L, Hui D. 2016. Unsupervised SAR image change detection based on SIFT keypoints and region information. IEEE. 13(2):931–935. IEEE Geoscience and Remote Sensing Letters.

Yawalkar PM, Kharat MU, Gumaste SV. 2018.segmentation of multiple touching hand written Devanagari compound characters. Chapter 8, IGI Global; p. 140–163

Internet from 18-Jul-2010 12:00AM. [accessed 2019 May 1]. www.gisteam.de-

Internet from 06-Nov-2012 12:00AM. [accessed 2019 May 1]. www.ictbm.org-

Internet from 30-Oct-2013 12:00AM. [accessed 2019 May 1]. www.aishack.in-

Internet from 27-Nov-2018 12:00AM. [accessed 2019 May 1]. ijarcsee.org